STATE RESEARCH CENTER OF RUSSIA

INSTITUTE FOR HIGH ENERGY PHYSICS

IHEP 2001-2

A.G.Abramov, N.A.Galyaev, V.I.Garkusha, J.Hylen[1], F.N.Novoskoltsev,
A.D.Ryabov, V.G.Zarucheisky

BEAM OPTICS AND TARGET CONCEPTUAL DESIGNS FOR THE NUMI PROJECT

Submitted to *Nuclear Instruments and Methods*

---

[1] Fermi National Accelerator Laboratory, Batavia, Illinois 60510, USA

Protvino 2001

UDK 539.12.183 M–24

Abstract

Abramov A.G. et al. Beam Optics and Target Conceptual Designs for the NuMI Project: IHEP Preprint 2001-2. – Protvino, 2001. – p. 22, figs. 16, tables 7, refs.: 24.

A summary is presented of the conceptual design of the focusing system for the Neutrinos at the Main Injector (NuMI) beamline at Fermilab. The 120 GeV primary proton beam with intensity of 4×10^{13} protons per 1.9 s from the Main Injector will be used to produce pions in a graphite target. Two 200 kA pulsed horns will be used to magnetically focus the resulting pion beam down a drift space where pions will decay to muon-neutrinos. The MINOS experiment will use the neutrino beam together with two detectors, one located on the Fermilab site and the other 735 km away in the Soudan mine in Minnesota, to study neutrino oscillation phenomena. Several neutrino beam optics configurations and target designs have been studied with the goal of producing a facility with high efficiency while retaining flexibility.

Work supported by the U.S. Department of Energy under contract № DE–AC02–76CH03000.

Аннотация

Абрамов А.Г. и др. Разработка оптики пучков и конструкции мишеней для проекта NuMI: Препринт ИФВЭ 2001-2. – Протвино, 2001. – 22 с., 16 рис., 7 табл., библиогр.: 24.

Представлены результаты концептуальной проработки фокусирующей системы для нейтринных пучков (NuMI) на главном инжекторе ФНАЛ. Выведенный из ускорителя протонный пучок с энергией 120 ГэВ и интенсивностью 4×10^{13} протонов в импульсе каждые 1.9 с будет использоваться для рождения пионов в графитовой мишени. Фокусировка пучка в направлении распадного участка, где пионы распадаются на мюоны и нейтирино, будет осуществляться двумя магнитными импульсными горнами с током 200 кА. Полученный нейтринный пучок наряду с двумя детекторами, расположенными один в ФНАЛ, а второй на расстоянии 735 км от ФНАЛ в шахте на территории штата Миннесота, будут использованы для изучения осцилляций нейтрино в эксперименте MINOS. Несколько вариантов оптики пучка и конструкции мишени было проработано для достижения высокой эффективности и, одновременно, гибкости фокусирующей системы.

Работа выполнена при финансовой поддержке Министерства энергетики США по контракту № DE–AC02–76CH03000.

1. Introduction

The MINOS experiment [1] is designed to explore the region of neutrino oscillation parameter space indicated by atmospheric neutrino experiments. Depending on what the neutrino mass-difference actually turns out to be at the given distance from Fermilab to Soudan, the MINOS experiment will need neutrinos in the energy range from 1 to 20 GeV. The lower end of this range is where it is expected, the ν_μ disappearance oscillation signal will be the largest, while the higher energies would be required to get above the τ production threshold for a ν_τ appearance signal. A system of currently known focusing elements cannot provide a high efficiency of focusing simultaneously over this whole energy range. Also, having a narrower energy band of neutrinos can be advantageous in reducing the background from the non-oscillation region. Thus, the ability to relatively easily tune a narrower energy-band focusing system over the 1 to 20 GeV energy range is an important requirement for the beam optics design.

The proposed focusing system uses magnetic horns, which are the most extensively employed focusing elements in existing [2,3] and preceding [4,5,6] neutrino beamlines. A pulsed current running down the inner and back the outer of two co-axial conductors produces a toroidal magnetic field between them. This field is used for focusing and at the same time for sign selection of charged pions. The pions enter and exit the horn by passing through the inner conductor, and the shape of inner conductor should be thoroughly optimized to provide high angular and momentum acceptances in the required energy range. A focusing system may consist of 1, 2 or 3 magnetic horns. The second and third horns are often referred to as "reflectors". As a rule, a single-horn focusing system is about 50% efficient in comparison with a two-horn system. On the other hand, the gain adding a third horn can be marginal since the additional focusing efficiency is balanced against absorption of pions by the horn material (especially for a focusing system located inside the target hall with the length which is significantly smaller than the total length of the decay region).

2. General Description of Beam Optics Designs

2.1. Wide Band Beam Configurations

A flexible neutrino beam optics, which may be tuned to different neutrino energy ranges, has been designed for NuMI. This focusing system (labeled as PH2) consists of two 3 m long magnetic horns with parabolic shaped inner conductors. Although the focusing is continuously variable, three tunes which jointly span the energy range from 1 to 24 GeV have been chosen for further study. These are labeled the low energy (LE), medium energy (ME) and high energy (HE) wide band neutrino beams (WBB). These beam configurations use the same horns and power supply system, but different targets and different positions of the second horn (Figure 1). The current in the horns, which are powered in series, is equal to 200 kA for all beam configurations.

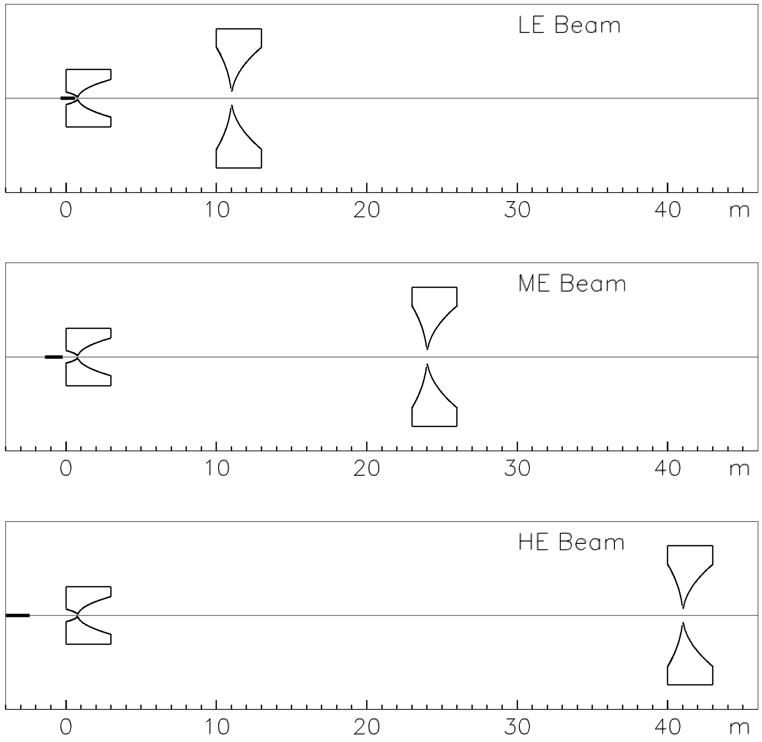

Fig. 1. Layouts of three different configurations of the PH2 wide band neutrino beam ($Z = 0$ corresponds to the upstream end of the first horn).

The basis of the design can be understood from a few fundamental approximations, although the optimization and detailed design requires extensive Monte Carlo calculations. First, we note that in pion decays where the neutrino goes forward to the detector, the neutrino energy is approximately 42% of the pion energy. So, by selecting which momentum pions we focus, we are selecting the resulting neutrino energy. For a given momentum and distance from a target, the required transverse momentum ($p_\perp$) kick from the horn to focus the pion parallel to the beam axis grows linearly with radius. Since the magnetic field is falling as $1/R$, the path length through the horn is required to grow as R^2, i.e. the inner conductor should be parabolic. In this a thin lens approximation, the focal length of the horn is proportional to the momentum, and the energy of the neutrino beam can be selected by varying the distance of the target to the horn. That this maintains a reasonable efficiency for a real horn depends on the fact that pion production peaks at $p_\perp \sim 0.3$ GeV/c for all pion momenta, so that the required inner and outer radii of the horn for a good acceptance remains reasonably constant. The same acceptance constraint is the reason for producing a lower energy beam by lowering the horn current does not work.

The second horn is located at a point where over and under focused pions have had a chance to drift out to a larger radius. Again, the angles are smaller for higher momentum tunes, so the distance between horns should be greater for optimal performance.

Tunes intermediate between the three studied can be easily achieved with the PH2 system at NuMI, but more extreme tunes are problematic. While the target to first horn distance can be increased to produce an even higher energy beam, the length of the NuMI target hall prevents any increase in the distance between the horns, leading to non-optimal performance. Tuning to lower energy is also limited, since for the LE configuration, the 2/3 target length already extends inside the first horn. Thus, to obtain an even lower energy neutrino beam would require a different, specialized horn.

The shapes of the horn inner conductors (see Section 4) were originally optimized for producing a neutrino beam mainly in the ME (2–12 GeV) range [7] and more recently somewhat modified in favor of the LE (1–6 GeV) beam [8]. The HE beam configuration (4–24 GeV) covers the remaining part of the total desired energy range. Both ME and HE configurations provide neutrinos with energy exceeding the threshold for τ-lepton production.

Once the target location is fixed to give the desired energy, target parameters are chosen for each beam configuration to maximize the ν_μ charged current event rate in the far detector. Graphite and beryllium were chosen as candidate target materials. The WBB targets are 1.9–2.4 interaction lengths, implying about 90% of primary protons interact. The target is in the shape of a long narrow fin, to maximize the escape of pions out the sides before reinteracting. To decrease the absorption of secondaries contributing to the high energy part of the neutrino spectrum, the average densities of the ME and HE targets are reduced to 0.81–0.85 and 0.61–0.64 respectively of the nominal material density ($\rho_\circ$) by the introduction of air gaps between target segments. The difference in optimal densities is due to the increased depth of focus in higher energy configurations of the horn system, as well as the fact that higher energy secondaries are produced at smaller angles. The LE target uses the maximum possible density, which is $\sim 0.96\rho_\circ$ after the introduction of multiple short segments and rounded segment corners to relieve stress. WBB target designs are described in detail in Section 5.

2.2. Narrow Band Beam Configuration

The two magnetic horns in the WBB focusing system can also be used to produce a narrow band beam (NBB) [9,10]. With the addition of dipoles, collimators and a primary proton beam absorber[1] one can obtain a beam of secondaries with relatively small $\Delta p/p$ and angular divergence. The main advantage of this NBB optics design is its use of the same focusing devices and power supply system for both wide and narrow band beams and a simple change between two types of neutrino beams.

Figure 2 shows the layout of a NBB optics design compatible with the HE configuration of the WBB focusing system described above. Because of the azimuthal symmetry of horns, either of the two transverse directions may be chosen as a bending plane for B1÷B3 dipoles. There are two possible ways to tune this NBB optics to various momenta:

- by changing the location of the target and scaling dipole currents, while keeping the horn current constant;

---

[1] The conceptual design of the NBB primary beam absorber [7,10] is in many respects similar to that of the beam absorber for the Fermilab Main Injector abort system [11].

- by varying the current in each horn and scaling currents in dipoles, keeping the target at a fixed position.

The first way provides the highest acceptance for all tunes, while the second one may simplify tuning the beam to various momenta. A mechanism to supply different currents to each horn are needed in the second case, either with separate power supplies or a shunt. In both cases positions of horns and elements of the momentum selection bends remain unchanged. To obtain narrow band beams with momenta of the parent particle from 10 to 40 GeV/c, the horn current does not exceed the 200 kA used for the WBB.

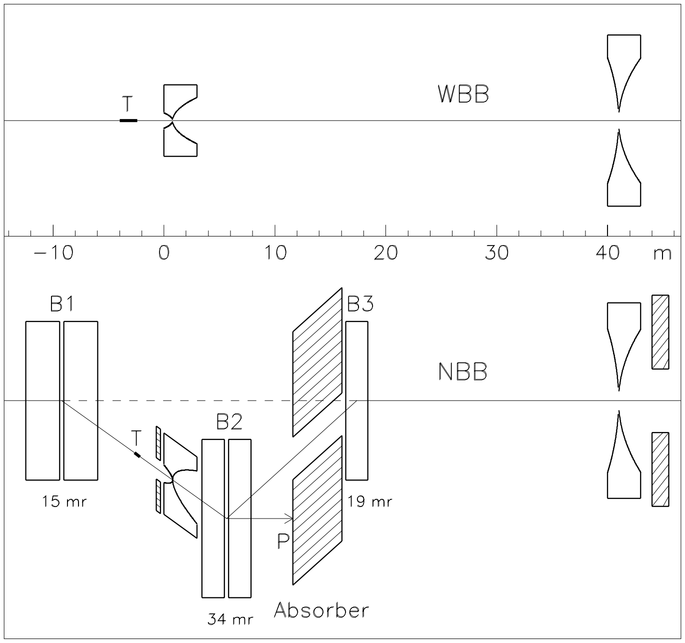

Fig. 2. The layout of the PH2 narrow band beam in comparison with that for the HE confi- guration of a WBB.

Although low density WBB targets may be used for the highest energy tunes of the NBB focusing system, a 0.5 m length target with an average density of $\sim 0.9\rho_\circ$ appears suitable for all NBB tunes. The details of a NBB target design were not considered at this stage, but to a great extent they are the same as for WBB targets.

3. Neutrino Beam Spectra and Event Rates

3.1. Neutrino Beam Simulation

Two neutrino beam simulation programs, which differ in time consumption and the number of effects included in the simulation, have been used to calculate neutrino flux in the detector acceptance.

HALO, originally developed at CERN [12] for the calculations of the muon background in charged particle beams, was modified to produce weighted neutrinos in the detector acceptance. A new focusing element, magnetic horn, was inserted in this program, and a more realistic simulation of primary proton interactions in the target was added. $\pi^\pm$ and $K^\pm$ are generated by the Monte Carlo method, and decay weights and acceptances for neutrinos are calculated at multiple locations as the particles are tracked along the beam line. Absorption and scattering of hadrons in the target and in the inner conductors of the horns are taken into account, but secondary particles are not generated. The program's speed allows many design variations to be checked.

GNuMI, developed at Fermilab specifically for NuMI beam design [13], is based on the GEANT package and simulates a wide range of physical effects. It includes production of secondaries in collimators, horn conductors, and decay pipe walls. More types of decay chains of charged and neutral particles contributing to the neutrino flux in the detector are followed, making it suitable for calculation of e.g. ν_e backgrounds. Subtleties such as the effect of muon polarization have been included. This allows studies which are beyond HALO's capabilities, although the significantly larger (several orders of magnitude) time consumption severely limits the number of beamline variants that can be simulated.

Use of two such different computer programs is required for an optimum approach to neutrino beam optics design. The first one allows optimization of a focusing system with a large number of parameters and for an estimation of effects on neutrino spectra of systematic errors in a focusing system, while the second one is very important for background calculations in both wide and narrow band neutrino beams and for neutrino beam simulations taking into account some details of horn and target designs.

Neutrino event rates in both near and far detectors, located at 1.05 km and 735 km downstream the target respectively, were calculated per one kiloton of detector for a year, which assumes 3.7×10^{20} protons on target. The total length of the decay region is equal to 725 m including the 50 m length target hall and the 675 m length and 1 m radius decay pipe. Both WBB and NBB results assume graphite as the target material. Due to uncertainties in hadron production cross sections, a systematic error of order 20% should be applied to the ν_μ rates.

3.2. Wide Band Neutrino Beams

Energy spectra of ν_μ Charged Current (CC) events in the far detector are shown in Figure 3 for the WBB configurations of the PH2 focusing system. The optics layout, event rates and backgrounds are summarized in Table 1. The results shown are from GNuMI.

Table 1: Target parameters and neutrino CC event rates in the far detector for different configurations of the PH2 focusing system. Target positions are given with respect to the upstream end of the first horn (see Figure 1). ν_τ CC rates are calculated assuming oscillations with $\sin^2 2\theta = 1$.

Beam configuration	LE	ME	HE
Target length, m	0.94	1.20	1.60
Target $Z_{upstream}$, m	–0.34	–1.40	–4.00
Target average density, g/cm^3	1.74	1.54	1.16
ν_μ CC events/kton/year	496	1424	2936
FAR/NEAR ratio for ν_μ CC	1.5×10^{-6}	1.2×10^{-6}	1.1×10^{-6}
Fraction of: $\tilde{\nu_\mu}$ events	10.2 %	3.45 %	1.10 %
ν_e events	1.05 %	0.84 %	0.60 %
$\tilde{\nu_e}$ events	0.21 %	0.08 %	0.03 %
ν_τ CC events/kton/year:			
for $\Delta m^2 = 0.01$	25.2	134	277
for $\Delta m^2 = 0.001$	0.56	2.6	3.8

The LE beam configuration provides a factor of 9 increase of ν_μ CC events in the energy range 1–6 GeV compared to having no horns for the given decay region. Corresponding values for the ME (2–12 GeV) and HE (4–24 GeV) beam configurations are equal to 14 and 17 respectively. One expects that this focusing efficiency is somewhat smaller than that obtainable with a focusing system optimized for one particular energy range.

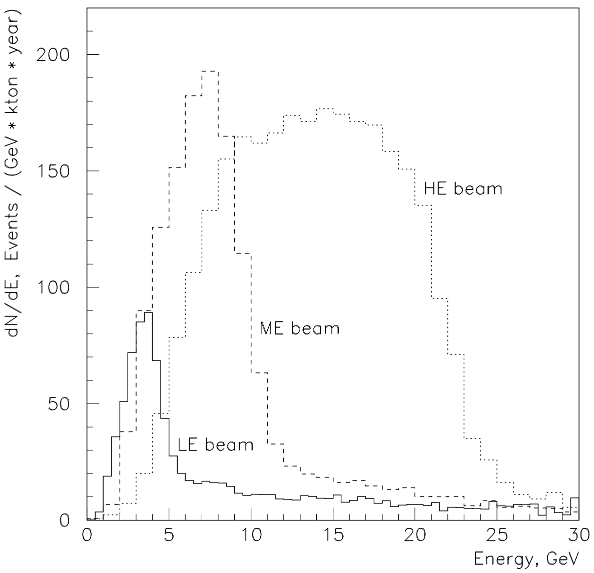

Fig. 3. Energy spectra of ν_μ CC events in the far detector for three WBB configurations of the PH2 focusing system.

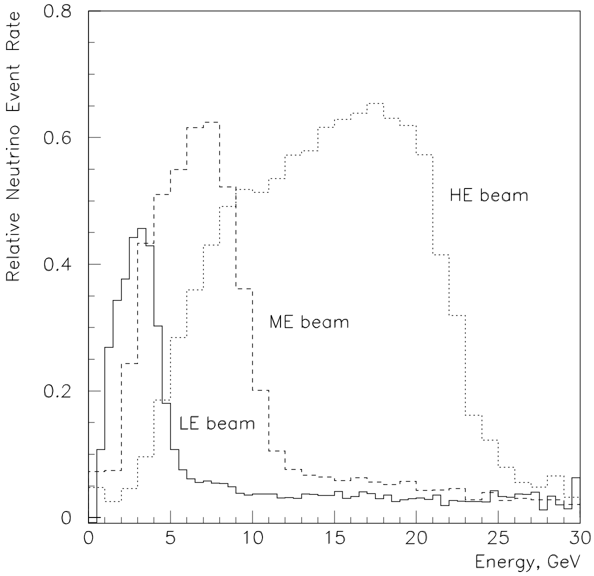

Fig. 4. Energy spectra of ν_μ CC events in the far detector for the PH2 focusing system divided by spectra provided by a perfect focusing system in the same decay region.

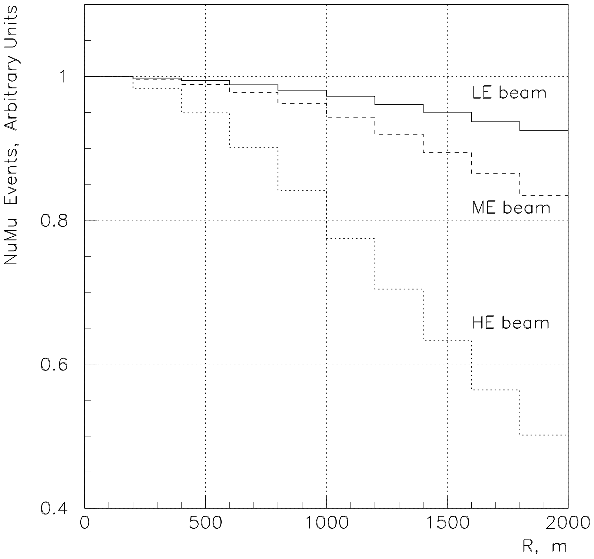

Fig. 5. Radial distributions of ν_μ CC events in the far detector.

Another performance evaluation of the focusing system is provided by a comparison of spectra achieved with a spectrum from an ideal focusing system. We define perfect focusing as a system where all neutrino parents are focused directly towards the detector, without absorption in focusing elements, but retaining the 725 m length decay region. In the corresponding neutrino energy ranges the LE, ME and HE configurations of the PH2 focusing system deliver 27%, 41% and 49% of the perfect focusing event rate (Figure 4).

Figure 5 shows the radial distribution of ν_μ CC events at the far detector location. The distribution is flat over an area significantly larger than the 4 m far detector radius. Beam to detector alignment within 0.2 mrad is sufficient to obtain the maximum possible neutrino event rate in the far detector, and is also sufficient to keep spectral distortions to a couple percent.

The largest background in the ν_μ beam is $\tilde{\nu_\mu}$, but $\tilde{\nu_\mu}$ CC events are relatively easily identifiable in the MINOS detector and do not compromise the oscillation measurements. The large increase of the relative $\tilde{\nu_\mu}$ background in the LE beam (10.2%) compared to that in the HE beam (1.1%) can be understood from the reduced geometric acceptance for defocusing negative pions near the beam axis combined with the lower rate of ν_μ.

The $(\nu_e+\tilde{\nu_e})$ component of the neutrino beam is an important background for ν_e appearance searches. This component also tends to be larger for neutrino beams with smaller energies. The main contributors to this background (81% in the ME beam) are $K^+\rightarrow\pi^\circ e^+\nu_e$ and $\mu^+\rightarrow e^+\nu_e\tilde{\nu_\mu}$ decays. Similar to other neutrino beams [14], the ν_e from K^+ decays have a broad energy distribution and are produced mostly in the first part of the decay pipe, while the ν_e from μ^+ decays are concentrated in the energy range of useful ν_μ neutrinos and are produced almost uniformly along the decay pipe (Figure 6).

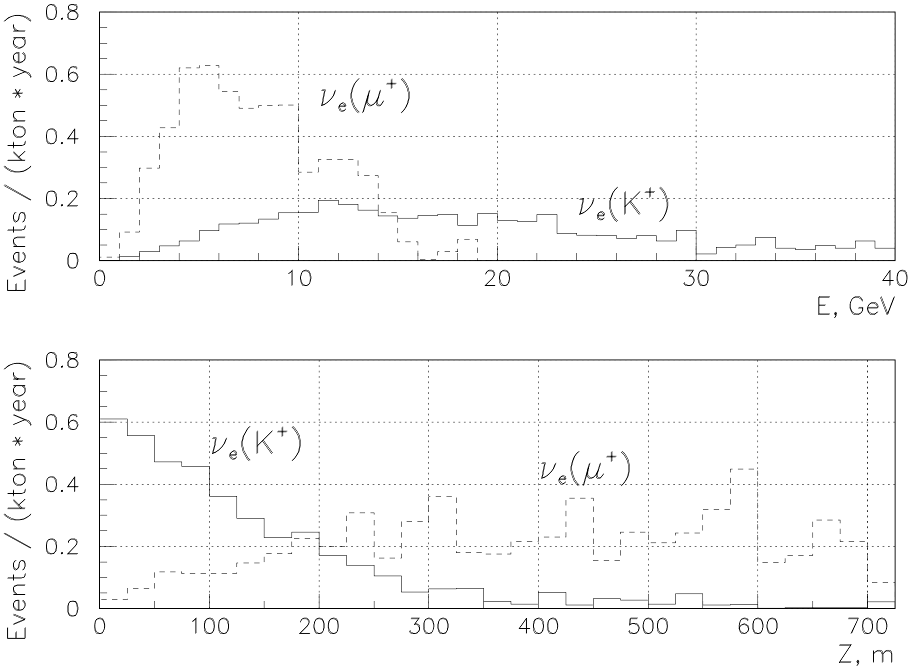

Fig. 6. Energy spectra of ν_e CC events in the far detector (top) and distributions of their decay points along the decay pipe (bottom) for the ME beam.

Neutral Current interactions from ν_μ in the high energy tail of the LE beam produce a background in some oscillation tests. This tail may be suppressed by placing a beam plug near the axis of the focusing system to absorb most of the high energy parents. Figure 7 illustrates the effect of a 1.5 m long, 18.5 mm radius graphite plug located close to the downstream end of the first horn. This beam plug gives a factor of 2.6 reduction in the high energy part of the neutrino spectrum with only a minor impact on the low energy part of the spectrum. The beam plug also cuts in half the number of $\tilde{\nu_\mu}$ CC events in the far detector, but the fraction of $(\nu_e+\tilde{\nu_e})$ events remains almost unchanged.

The use of a lower primary beam energy is another way to cut down the high energy tail. However, a correspondingly higher intensity of primary protons is required to obtain the same event rate in the peak.

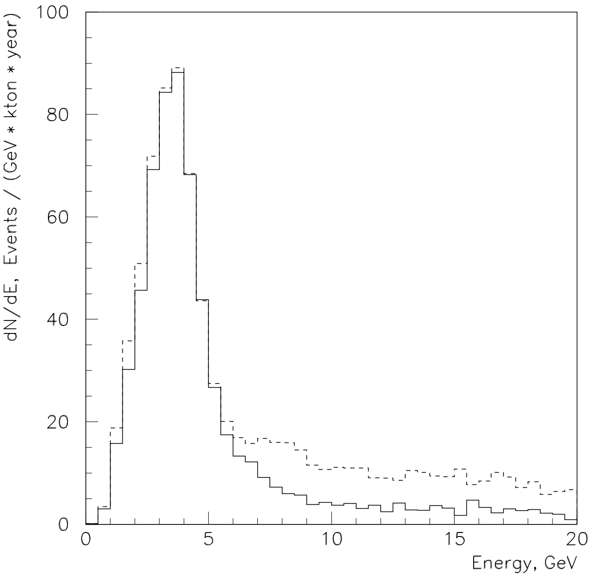

Fig. 7. Energy spectra of ν_μ CC events in the far detector for the LE beam with the beam plug (solid line) and without it (dashed line).

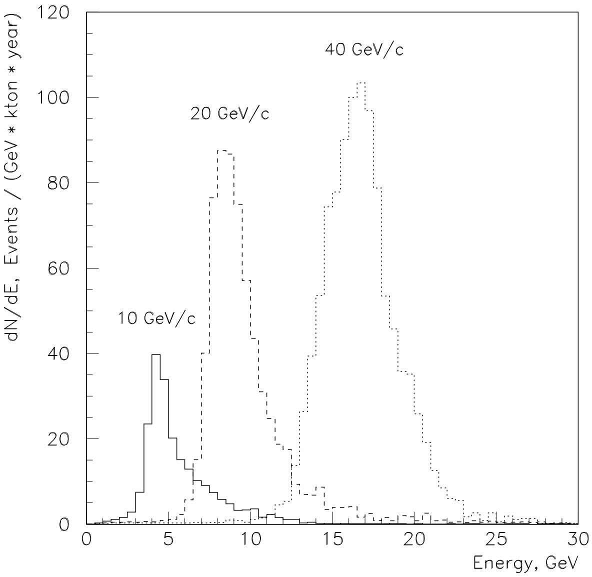

Fig. 8. Energy spectra of ν_μ CC events in the far detector for three different tunes of the NBB configuration with the 0.5 m length target.

3.3. Narrow Band Neutrino Beams

Energy spectra of ν_μ CC events in the far detector for three different tunes of the PH2 NBB configuration are shown in Figure 8. Total ν_μ CC event rates for these spectra are given in Table 2. Although the tunes for parent particle momenta smaller than 10 and larger than 40 GeV/c are not possible in this configuration, any intermediate tune may be realized by corresponding adjustment of the target location and dipole currents, keeping the current in both horns at its nominal value of 200 kA (see Section 2).

Table 2: Total ν_μ CC event rates in the far detector for three NBB tunes. Positions of the 0.5 m long and ~0.9$\rho_\circ$ average density target are given with respect to the upstream end of the first horn.

NBB tune, GeV/c	10	20	40
Target $Z_{upstream}$, m	–1.0	–2.1	–3.3
Dipole field, kGs·m	17.65	35.31	70.62
ν_μ CC events/kton/year	110	330	540

Longer, lower density targets may be used for higher energy NBB tunes. In particular, the 1.6 m long target with an average density of 0.64$\rho_\circ$ (the HE WBB target) gives in case of the 40 GeV/c tune a ~40% increase of the total neutrino rate with respect to the 0.5 m long target. The use of a long target does not cause noticeable changes in NBB backgrounds.

For the use in a τ appearance analysis with the MINOS detector, minimization of the NBB low energy side tail is crucial. For the 40 GeV/c tune of the PH2 narrow band beam with 0.5 m long target the ratio of ν_μ CC events with $E_\nu < 10$ GeV to the total number of events in the far detector is 0.67%. The low energy ν_μ's are mainly from $\pi^+(K^+) \rightarrow \mu^+\nu_\mu$ decays, and their source locations are broken down in Table 3.

Table 3: ν_μ CC events with $E_\nu < 10$ GeV in the far detector (the low energy tail of neutrino spectrum) for the 40 GeV/c tune of the NBB.

Source of neutrino parents	Neutrino parents decays from:		
	Foc. system $Z < 50$ m	Decay pipe $50 < Z < 725$ m	Whole beam $Z < 725$ m
Interactions of primary protons in the target	2.48	0.14	2.62
Interactions of secondaries in horns, collimators and decay pipe walls	0.34	0.68	1.02
All sources	2.82	0.82	3.64

The 3/4 low energy tail comes from decays occurring in the focusing system, especially in the momentum selection part at $Z < 20$ m (see Figure 2). Shortening this part of the focusing system, an increase of bend angles in dipoles and variations of apertures and materials used in collimators may be considered as possible steps to further reduce the number of low energy neutrinos.

The fraction of ν_e CC events in the far detector is equal to 0.37% and comes almost entirely from μ^+ and K^+ three-body decays in the decay pipe. The 0.27% fraction of $\tilde{\nu_\mu}$ CC events has roughly equal contributions from π^-, K^- decays in the focusing system (before the momentum selection collimator) and from μ^+ decays in the decay pipe. $\tilde{\nu_e}$'s comprise less than 0.1% of the beam.

4. Parabolic Horns

The shape of the inner conductors and currents in the horns of the PH2 focusing system were optimized to maximize the number of neutrino events in the far detector with energy less than 12 GeV (LE and ME beams), while taking into account the possible use of these horns for neutrino beams with higher energies (HE beam).

Cross–sections of both horns are schematically shown in Figure 9 and their numerical descriptions are listed in Table 4. The inner conductor of each horn consists of two paraboloids connected together by a small neck. The outer surface of an inner conductor is described by $R = \sqrt{|Z - Z_\circ|/P}$, where R is the radius, Z is the distance from the upstream end of the horn, P is the parabolic parameter, and $Z_\circ$ is where the parabola would intercept the beam axis. The toroidal magnetic field is produced in the volume between the co-axial inner and outer conductors by a 200 kA pulsed current. In spite of some loss in focusing efficiency for high energy secondaries, the inner radii of the horn necks were made large enough to prevent heating of the necks by remnants of the primary proton beam emerging from the target and by possible small mis-steerings of the proton beam. (Baffle collimators upstream of the target prevent large primary beam mis-steerings from reaching the horns).

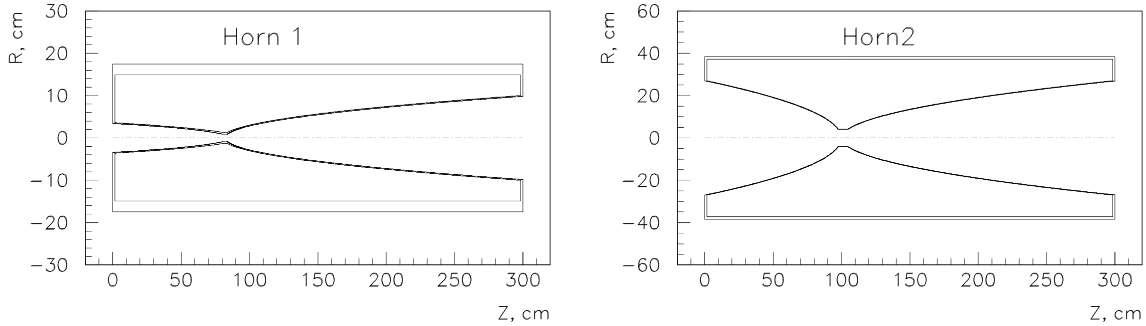

Fig. 9. Cross–sections of the PH2 horns.

Table 4: Geometrical parameters of PH2 horns.

Horn parameters	Horn1		Horn2	
	1-st part	2-nd part	1-st part	2-nd part
Extent in Z, cm	0.–80.	83.98–300.	0.–97.62	104.80–300.
Parabolic parameter P, cm^{-1}	7.048	2.185	0.135	0.272
Parabola intercept $Z_\circ$, cm	92.85	80.00	100.	100.
R_{in} of the neck, cm	0.90		4.0	
R_{out} of the neck, cm	1.35		4.2	
R_{in} of the outer conductor, cm	14.92		37.15	
R_{out} of the outer conductor, cm	17.46		38.42	

The thickness of the inner conductors in the horns, which should be minimized to reduce absorption and scattering of secondaries in the conductor material, must also be thick enough to withstand repetitive thermal and magnetic stresses over at least 10^7 current pulses. The thickness of the inner conductor in the first horn is 4.5 mm in the neck region. Moving away from the neck, the inner surface of the inner conductor follows an offset paraboloid, so that the thickness gradually decreases to 2 mm at $R = 2.63$ cm, whereafter the thickness remains constant. The thickness of the inner conductor in the second horn is equal to 2 mm along the whole length.

According to beam simulations, the decrease in neutrino event rate in the far detector due to the absorption of secondaries in inner conductor material is 16–17% for ME and HE beams and for neutrinos with $E_\nu < 6$ GeV in the LE beam. (Total absorption loss of neutrino events in the LE beam is 12%). Multiple Coulomb scattering causes another 2–3% decrease in the event rate, so that the overall loss due to inner conductor material is nearly 20%.

The average power deposited in the inner conductors due to the Joule heat load is approximately 17 kW and 5.2 kW for the first and second horns, respectively, and the per pulse temperature rise in the neck region of the first horn reaches $\sim$23°C[2]. Water will be continuously sprayed on the inner conductors to remove this heat. The heat load from energy deposition by secondary particles in the inner conductor material is significantly smaller than the electrical heat load, being 1.6 kW for the first horn and 0.15 kW for the second one for ME beam.

Heating and the resulting stress of the inner conductors, as well as requirements for the horn cooling system and power supply, would be decreased for a focusing system with a smaller current. To keep the same value of $\int Bdl$ as required by a "point to parallel" focusing of parent particles ($\sim$1.3 Tesla-meters for parents with initial $p_\perp = 0.4$ GeV/c), a decrease of horn current should be compensated by an increase in horn size. An estimate of the size versus current relation can be made based on the solution of the particle motion equation in a toroidal magnetic field $B \propto 1/R$

$$\frac{d^2R}{dZ^2} + \frac{k}{R} = 0,$$

where $k = 6 \times 10^{-5} I/p$, I is the current (kA) and p is the particle momentum (GeV/c).

As shown in Figure 10, for higher energy neutrino beams (e.g. the HE configuration of the NuMI beam or the CNGS beam at CERN [15]), the necessary length of the magnetic field region varies inversely with current, while the transverse size remains almost unchanged. However, in the energy range of a few GeV (e.g. the LE configuration of the NuMI beam), a reduction in

---

[2] The horns are designed for a 5.2 ms half-sine wave current pulse to accommodate a 1 ms spill of resonantly extracted primary beam, and this value is used for heating calculations. The actual mode of operation for initial running will be a 2.6 ms half-sine wave with the 8.6 μs single turn extracted spill.

the current leads to rapid increases of the required length and transverse size of the magnetic field region. Thus, the use of horns with a current significantly smaller than 200 kA in focusing systems designed for a few GeV energy range is ineffective.

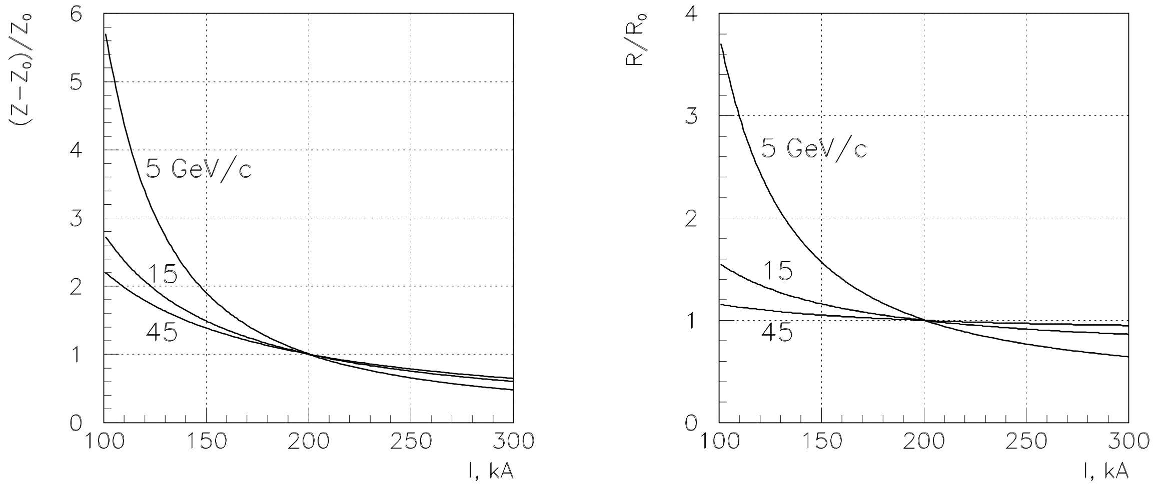

Fig. 10. The length (left) and transverse size (right) of the $B \propto 1/R$ field area as functions of current for "point to parallel" focusing of parent particles with $p_\perp = 0.4$ GeV/c and with various longitudinal momenta p. $R_\circ, Z_\circ$ and R, Z are input and output particle coordinates, respectively ($pR_\circ = p_\perp Z_\circ$). Each curve has been normalized to the point at 200 kA.

5. WBB Target Designs

5.1. General Approach

The choice of target material and size is a compromise between maximizing the neutrino event rate and achieving a reasonable reliability of target operation. The design goal is to have a target last 1 year ($\sim 10^7$ beam spills). Because of the large average power (1.6–2.6 kW) deposited in a target by the 120 GeV and 4×10^{13} protons per spill of the primary beam, a fin shape was chosen for the target, which allows conduction transference of the heat to a water cooling system. Optimization studies indicate an elliptical shape primary beam spot with relationships $\sigma_y \simeq 2\sigma_x$ and $d \simeq 4.5\sigma_x$ between primary beam spot sizes and the width of a target works well. Graphite ZXF–5Q from Poco Graphite, Inc. and beryllium S–65C from Brush Wellman, Inc. have been considered as possible target materials.

The targets for the ME and HE beams are conceptually the same. The differing focal length and depth of field of the focusing system and angles of maximum production of secondaries appropriate for the two cases only cause modest differences in length and average density of target material (see Table 1). To maximize the neutrino event rate, the LE target is placed with the 2/3 its length inside the first horn; therefore, the maximum transverse size of the target is limited by the internal diameter of the horn inner conductor at the downstream end of a target, and should be less than 40 mm. In this case most of the secondaries contributing to the neutrino event rate in the detector will cross through the sides of the target casing, which must thus be thin to minimize absorption.

The target casing allows for an inert atmosphere around the active part of the target, contains radioactive debris in case of target failure, and provides rigidity of the LE target/cooling-line structure. Due to the high power of the beam, the cooling system and target casing should be located outside the range of possible mis-steered primary proton beam. The possible beam trajectories are restricted to less than 9 mm radius by baffle horn-protection collimators; the only target components in this region are the fin, inert atmosphere, and thin beryllium end-windows.

5.2. ME Target Design

The general view of the ME target design is shown in Figure 11. The primary proton beam travels through the top of twelve 3.2 (4.1) mm wide and 100 mm long graphite (beryllium) plates, which are pushed by pressing the plates against the base plate [16]. The base plate contains cooling and water return channels. Two springs per the target plate provide ∼2 atm pressure. The distance from the fin tip to the cooling channel is minimized at the upstream end, where beam heating is maximum, but to prevent absorption of secondaries contributing to the neutrino flux, the fin extension increases continuously along the target length. Base and pressing plates are made of an aluminum alloy and anodized with 30 μm thick alumina. The alumina provides electrical isolation of the target fins, enabling charge-read-out (Budal [17]) monitoring of the primary beam interaction with each target plate.

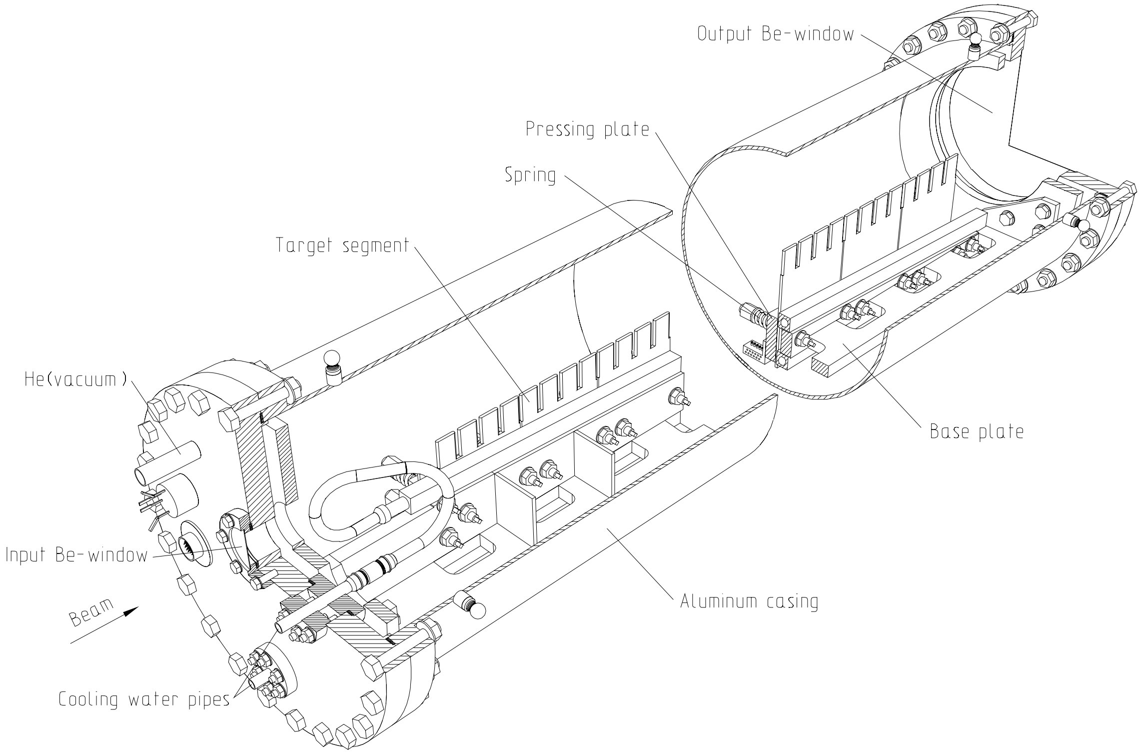

Fig. 11. General view of the ME target design.

To decrease quasi-static thermal stresses, cuts are machined in the upper part of each graphite plate, forming four 22 mm long, 30 mm high segments. For a beryllium target, each plate would consist of five 16.8 mm long segments. Segment corners are rounded with a radius equal to half the segment width, which significantly relieves stress concentrations.

The base plate is attached to a 7 mm thick, 290 mm diameter, ∼1.5 m long cylindrical aluminum casing. Two flanges with 0.5 mm thick beryllium windows separate the internal volume from the surrounding environment. The diameter of the upstream window is 45 mm; the diameter of the downstream window is determined by the maximal angle of secondaries accepted by the focusing system and should not be less than 120 mm. To prevent contact of the target material with air, the casing is evacuated or filled with helium or nitrogen. Using vacuum inside the target casing modestly improves the charge-read-out monitoring signal, and may be prefered during target alignment in the beam line. During normal operation, a helium fill has the advantage of improving the thermal contact between the target segments and base plate, and also relieves the stress on the beryllium windows.

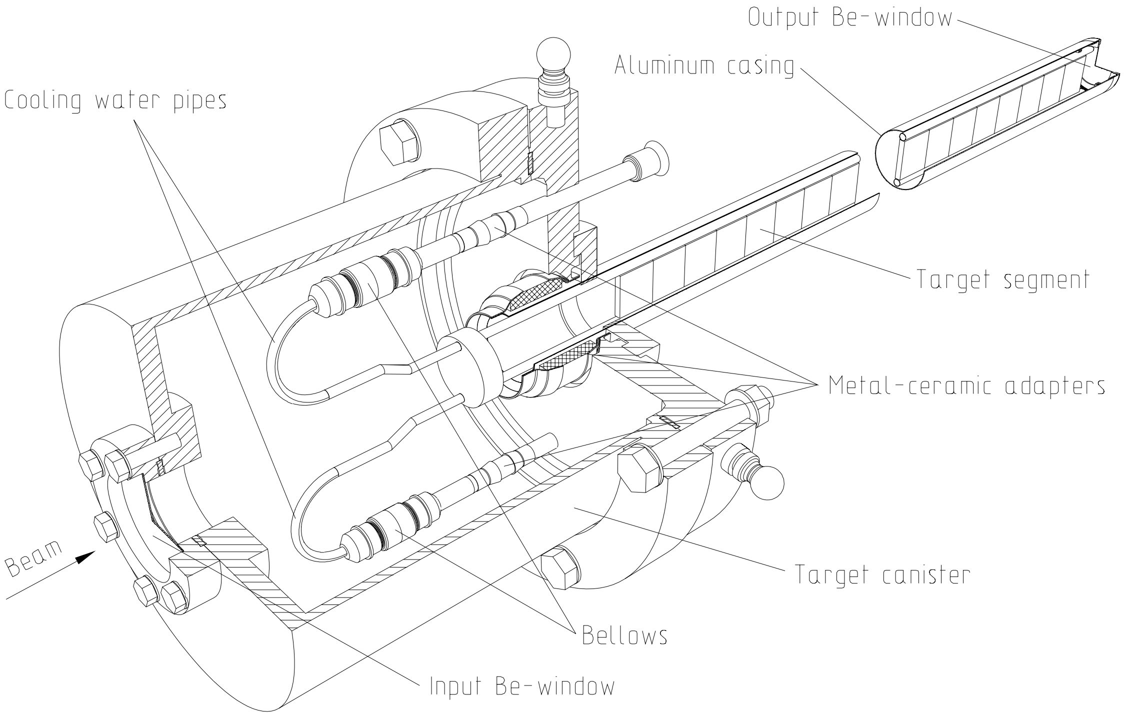

Fig. 12. General view of the LE target design.

5.3. LE Target Design

The general view of the LE target design is shown in Figure 12. The graphite (beryllium) target core is a row of 47 (56) segments, each 3.2 (4.1) mm wide, 20 mm high, and 20 mm (16.5 mm) long [18]. As in the ME target design, the corners of each segment are rounded with the radius equal to half the segment width. To avoid contact between heated segments, they are separated by ∼0.3 mm gaps. The segments are soldered by means of a soft solder with a melting temperature of ∼300°C to two steel cooling pipes with external diameter 4.0 mm and wall thickness 0.2 mm.

The target core is inserted into a 0.4 mm thick 30 mm diameter aluminum casing, centered by three aluminum spacers. The spacers are anodized with 30 μm thick alumina to provide electrical insulation of the target core for charge-read-out monitoring. Because the downstream end of the LE target is located close (∼5 mm) to the inner conductor of the first horn, metal-ceramic adapters are used to isolate the target casing and water cooling pipes from ground, preventing an electrical break-down path. Two bellows prevent any forces on the metal-ceramic adapters which arise in the design during assembly or operation. The target canister with ConFlat flange, target casing, and two beryllium windows enclose an internal volume which is evacuated or filled with inert gas to protect the target material from oxidation.

The total length of the LE target unit is equal to ∼1.2 m. The target may be mounted onto the outer conductor of the first horn, or the target may have its own support module as in the ME and HE cases. In either case, the target casing is fixed only at its upstream end, and gravity will cause a 0.6–0.8 mm sag at the downstream end. This sag is small compared to the vertical size of target segments; consideration of sag was, in fact, one of the factors leading to the choice of a fin design for the LE target.

5.4. Results of Temperature and Quasi-Static Stress Calculations

The adiabatic temperature rise due to the heat load of a target material by the primary proton beam can be estimated as $\Delta T = D_e N / C_p \rho$, where D_e is the energy deposition density per incident proton, N is the number of protons per spill, and C_p and ρ are the specific heat and the density of the material. Quasi-static thermal stresses, which arise because of non-uniform and almost adiabatic[3] heating of a target material, are $S \propto \alpha E \Delta T = (\alpha E / C_p \rho) D_e N$, where α is the coefficient of thermal expansion and E is the modulus of elasticity (Table 5). Most of these material properties are temperature-dependent[4], and this was taken into account in temperature and stress calculations.

Table 5: Properties of target materials at a room temperature.

Material	Graphite	Beryllium
Grade	ZXF–5Q	S–65C
Melting temperature, °C	3600	1284
Density ρ, kg/m^3	1810	1820
Specific heat C_p, J/kg/K	714	1790
Coeff. of thermal expansion α, 1/K	8.1×10^{-6}	10.3×10^{-6}
Modulus of elasticity E, Pa	14.5×10^{9}	312×10^{9}
Thermal conductivity λ, W/m/K	70	199

The MARS code [21] was used to calculate the energy deposition in target materials, while the ANSYS code was used to calculate temperature and thermal stress distributions. Calculations of target temperatures were carried out under the following boundary conditions:

- the thermo-resistance between a target material and the base plate (cooling pipes for the LE target design) is assumed to be zero. The input temperature of cooling water is equal to 20°C;
- the heat transfer coefficient to water is equal to 10 kW/m^2/K;
- for thermal radiation, target segments have an emissivity of 1.0, and the ambient temperature is 20°C.

---

[3] For both materials the time of thermal diffusivity within dimensions of a beam spot is 10–20 times greater than the spill time ($\leq$1 ms) for resonant extraction of the primary beam. On the other hand, this time is significantly less than the beam repetition period (1.9 s), which excludes an accumulation of thermal stresses.

[4] The specific heat C_p and the product of the thermal expansion coefficient and the modulus of elasticity αE of the ZXF–5Q graphite increase by a factor of 2 and 1.3 respectively as the temperature increases from 20°C up to 500°C [19]. Similarly, for S–65C beryllium the above properties grow in this temperature range by a factor of ∼1.5 [20]. Thermal conductivities of graphite and beryllium decrease at 500°C to 0.7 and 0.55 of their room temperature values, respectively.

The steady-state temperatures of target segments are determined by the average power deposited in segments and design features of the cooling system. The LE target segments are significantly cooler than the ME target segments because they are cooled from both ends and the cooling pipes are located at rather small (∼10 mm) and constant distance from the beam axis. The longitudinal distribution of segment temperature in the LE target reflects closely the longitudinal distribution of average deposited power (Figure 13). In contrast, for the ME target, the increase in distance between the beam axis and cooling channel along the target (from ∼30 to ∼85 mm) leads to the situation where the temperature of segments in the middle ($Z \simeq 0.5$–0.6 m) is somewhat higher than the temperature of segments with the maximal power deposition ($Z \simeq 0.1$–0.2 m). Steady-state temperatures are reached in 30–50 proton spills for the ME target and in 4–5 spills for the LE target.

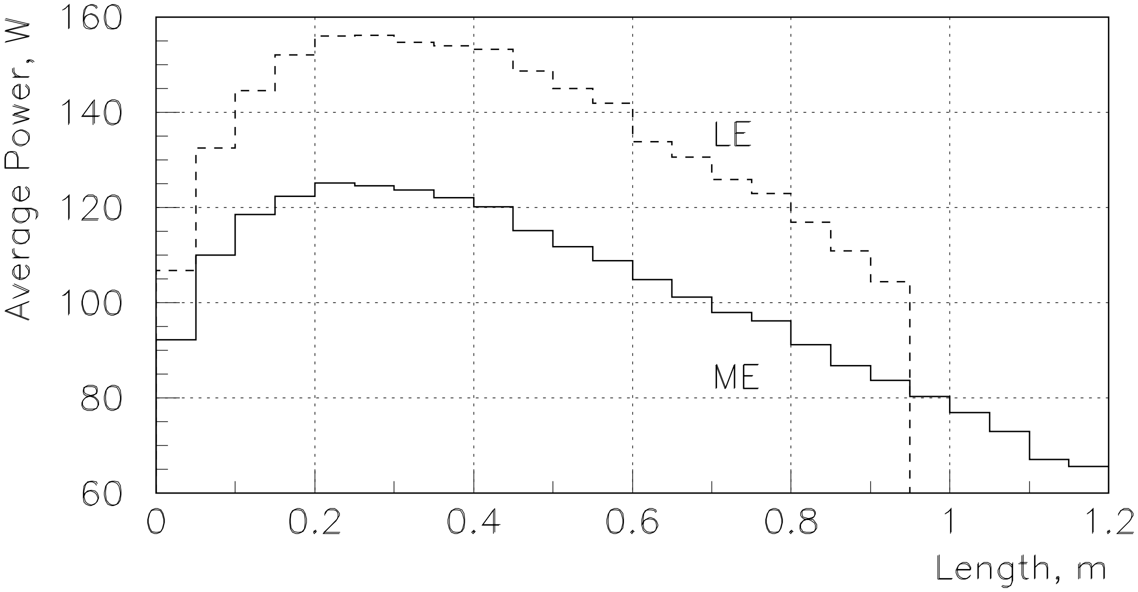

Fig. 13. Longitudinal distributions of power deposited in LE and ME graphite targets with average densities of 1.74 g/cm^3 and 1.54 g/cm^3, respectively.

Thermal stresses in a target material are mostly determined by the value of energy deposition density at the axis of the beam[5]. For both target materials considered the energy deposition density reaches maximum 0.1–0.15 m into the target and then decreases continuously, dropping at the downstream end to ∼0.3 of its maximum. Calculations of quasi-static thermal stresses show that:

- the target material is subjected to all-axis compression in the center and is stretched at lateral sides of target segments with significant stress concentration at non-rounded segment corners. Stresses grow with increasing segment length;
- maximal stresses arise in target segments with the highest energy deposition density. In these segments the equivalent (Von Mises) stresses at rounded corners of segments are somewhat larger than those in segment centers.

---

[5] Due to the temperature dependence of specific heat, the temperature rise and, consequently, the thermal stresses depend also on the initial temperature of the segment.

Steady-state temperatures and maximal equivalent stresses in target segments with the highest energy deposition density are given in Table 6. In addition Figure 14 gives distributions of temperature along the vertical axis of these segments for ME and LE graphite targets. We note that for the ME target, the hottest segment (with $T_{min} \sim 480°C$ and $T_{max} \sim 600°C$) has significantly less maximal stress than the upstream segment listed in Table 6.

Table 6: Temperatures at the beam axis and maximal quasi-static thermal stresses in target segments with the highest energy deposition density.

Target material	Graphite		Beryllium	
Primary beam spot size $\sigma_x \times \sigma_y$, mm^2	0.7×1.4		1.0×2.0	
Energy deposition density D_e, GeV/cm^3	0.092		0.045	
Width of the segment d, mm	3.2		4.1	
Target design	ME	LE	ME	LE
Segment length l, mm	22	20	16.8	16.5
Temperature after the beam spill T_{max}, °C	593	344	186	125
Temperature rise ΔT, °C	187	251	65	75
Temperature before the beam spill T_{min}, °C	406	93	121	50
Maximal equivalent stress S_{eq}, MPa	19.5	24.4	148	150

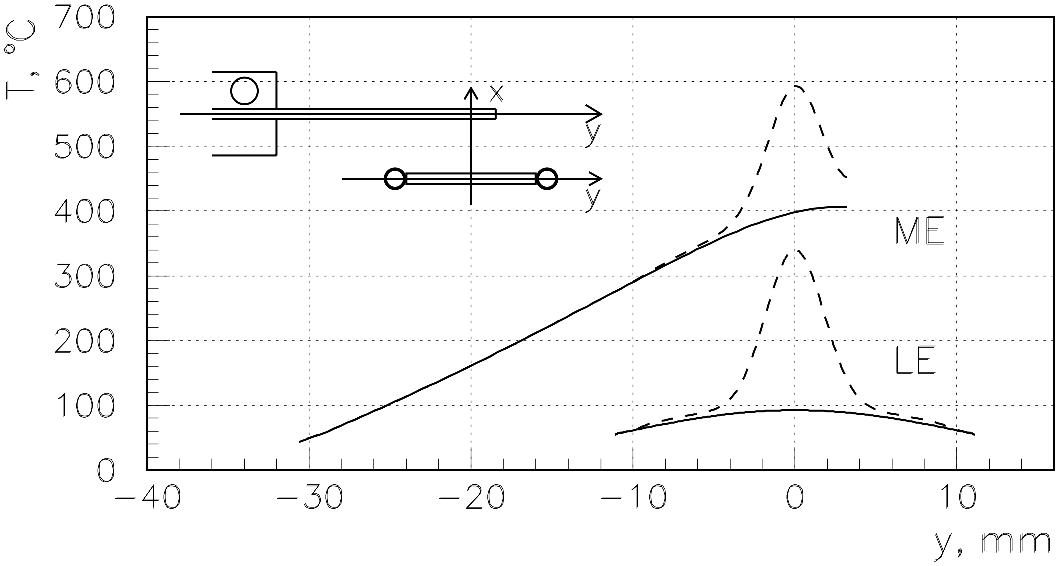

Fig. 14. Temperature distributions along the vertical axis of graphite target segments with the highest energy deposition density. Shown before (solid line) and after (dash line) the beam spill.

5.5. Dynamic Stresses in Targets in the case of Single Turn Extracted Primary Beam

Single turn extraction of primary protons from the Main Injector can be carried out cleanly, avoiding beam losses which are inherent to resonant extraction due to scattering on the electrostatic septa. Beam losses lead to activation of equipment in the extraction area and along the proton beam-line, and to an increase of shielding required around the beamline. Because of such considerations, NuMI now plans to begin operations using single turn extraction. This has in turn caused reexamination of the target designs.

The maximal dynamic stress in a target material, arising when heat loading occurs over very short time scales, is [22]

$$S_{max} \propto \begin{cases} \alpha E \Delta T & for \quad v_s \tau \leq l, \\ \alpha E \Delta T (l/v_s \tau) & for \quad v_s \tau \geq l, \end{cases}$$

where $v_s \simeq \sqrt{E/\rho}$ is the sound velocity, l is the length of a target segment and τ is the beam spill duration.

For resonant extraction of primary beam with $\tau \leq 1$ ms, the value of $v_s\tau$ is at least two orders of magnitude larger than the segment length l even for graphite with a sound velocity of $\sim$2.8 mm/μs (the sound velocity for the beryllium is equal to $\sim$13 mm/μs); thus quasi-static stress analysis is sufficient.

For a single turn extraction of primary beam with $\tau \simeq 8$ μs, $v_s\tau \sim 22$ mm nearly coincides with the length of the target segments. To check whether stress waves arising from these conditions do might destroy the material, calculations of dynamic stresses were made using ANSYS for LE and ME graphite targets[6].

Calculations of the energy deposition density in the graphite were carried out assuming the Gaussian distribution of the primary proton beam in both transverse directions. (The distribution expected for a resonant extraction is somewhat non-Gaussian). The maximal energy deposition density on the beam axis increased to 0.115 GeV/cm^3 for the $\sigma_x \times \sigma_y = 0.7 \times 1.4$ mm^2 proton beam spot size, in comparison with 0.092 GeV/cm^3 for a resonant extracted beam.

Time evolution of stresses at two points in the ME target segment with the highest energy deposition density are shown in Figure 15. The periods of oscillation of the stresses reflect the dimensions of the target segment, i.e. the wave lengths of S_{xx}, S_{yy} and S_{zz} oscillations agree well with double thickness, height and length of a segment, respectively. Due to coupling, the spectra of S_{yy} and S_{zz} stresses contain also the main frequency of S_{xx} oscillations. Coupling between neighboring target segments is not seen. The same behavior of dynamic stresses was also found in LE target calculations.

The average and maximal equivalent stresses at two points in the ME and LE target segments are given in Table 7. The increase of average equivalent stress over the resonant extraction case shown in Table 6 tracks to the first order increase of maximal energy deposition density from the change in a beam profile. Although the equivalent stress reaches its maximal value in the center of the target segment, the crucial point is at the rounded corner since the all-axis stretch in this point should be compared with the tensile strength limit of graphite, which is approximately half its compressive strength limit.

Table 7: The average and maximal equivalent stresses (MPa) for two target designs for a single turn extracted primary beam.

Position of the point on beam axis of a target segment	ME target		LE target	
	$\langle S_{eq} \rangle$	$(S_{eq})_{max}$	$\langle S_{eq} \rangle$	$(S_{eq})_{max}$
At the center (all-axis compression)	23.5	31.5	29.3	35.7
At the rounded corner (all-axis stretch)	21.9	25.3	27.3	33.4

---

[6] From stress calculations made for the 100 mm long beryllium rod CNGS beam target with $l/v_s\tau \simeq 0.8$ [15], one would expect that the lifetime of NuMI beryllium targets with $l/v_s\tau \simeq 0.16$ would be determined mostly by quasi-static thermal stresses.

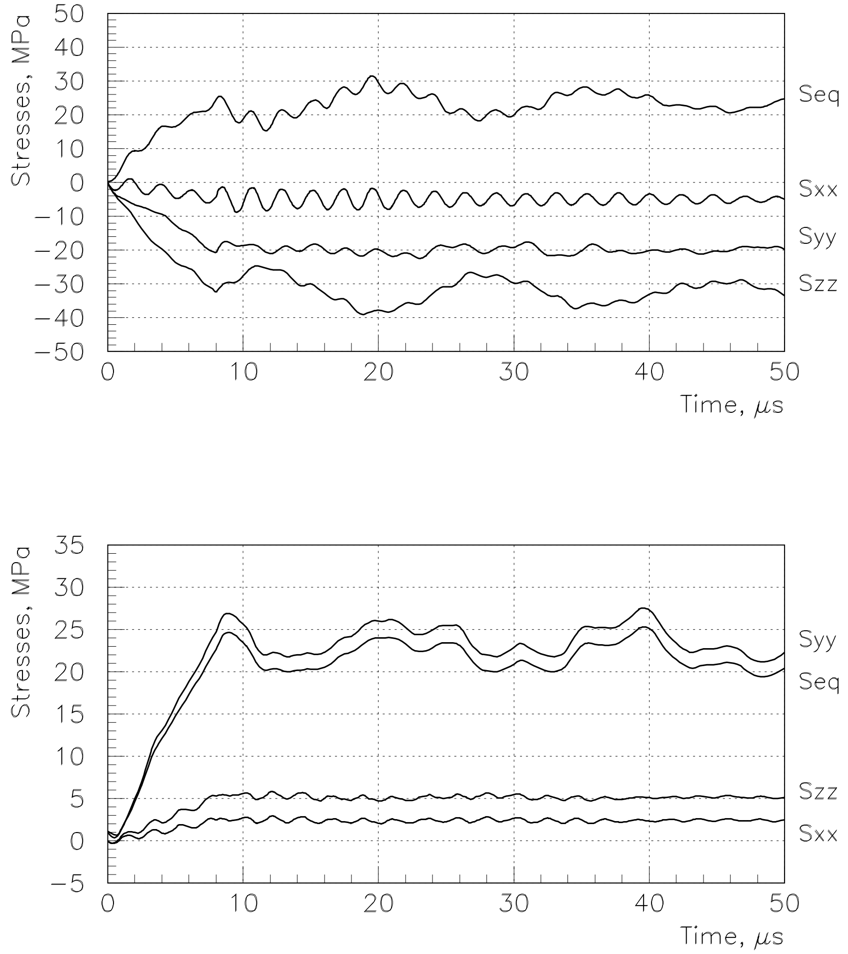

Fig. 15. Time evolution of stresses in the center (top) and at the rounded corner (bottom) of the ME graphite target segment. Both points are on the beam axis through the segment.

5.6. Target Lifetime

The high-cycle fatigue data for S–200F VHP (Vacuum Hot Pressed) beryllium grade show [20,23], that the 10^7 cycle fatigue endurance limit in both longitudinal and transverse directions is equal to 261 MPa, which coincides with the specified yield strength ($S_{0.2}$). The candidate chosen for NuMI targets, S–65C VHP grade, is purer than S–200F and has the best resistance to crack initiation and crack propagation at large thermal stresses. Assuming that fatigue properties of S–65C grade are similar to those of S–200F and that the fatigue endurance limit varies with temperature as the yield strength, the 10^7 cycle fatigue endurance limit for ME and LE targets may be estimated as 227 MPa and 240 MPa, respectively. The safety factor (the ratio of the fatigue endurance limit to the maximal equivalent stress occurring in target segments) is then ∼1.6.

No yield strength is specified for graphite since it is a brittle material. Unlike beryllium, the graphite has different compressive and tensile strength limits, which for ZXF–5Q grade with density of 1.81 g/cm^3 are equal to 210 MPa and 95 MPa, respectively. The strength of ZXF–5Q grows with temperature [19], but this increase occurs mainly above 1000°C and may be neglected below 600–700°C. Fatigue tests of graphite show [24] that, for cycles between zero stress and a tensile value, the 10^7 cycle fatigue endurance limit is in the range of 0.5–0.6 when expressed in terms of homologous stress (the ratio of an applied stress to the first cycle strength). Thus, the highest equivalent stresses in the ME and LE graphite target segments are respectively 2.7 and 2.1 times less than the fatigue endurance limit corresponding to one year operation of NuMI resonant extraction.

For a single turn extraction of the primary beam, the lifetime is determined by the maximal equivalent stress, which is 20–30% higher than the average value of equivalent stress (see Table 7). The safety factors are then 2.0 and 1.6 for ME and LE targets respectively for one year operation with a single turn extracted primary beam.

The safety factor needs to cover: (i) possible increase of the energy deposition density due to variation of primary beam focusing, (ii) inaccurates of the energy deposition and stress calculations, (iii) uncertainties in the fatigue analysis.

The design safety factor may be increased by an increase of σ_x, the primary beam width, with the corresponding increase of the segment width. This leads to a decrease of the energy deposition density with the subsequent decrease of the adiabatic temperature rise and thermal stresses in the target material. This, however, decreases a neutrino flux due to an extra absorption of secondaries in the target material. Simulations indicate that switching to 4.8 mm wide graphite plates to increase beam σ_x by a factor of 1.5 would decrease the neutrino event rate in the far detector by 2–3% for ME and LE beams and by 7–8% for the HE beam. The energy deposition density in target segments with a given width may also be decreased by a further stretching of the primary beam in the vertical direction ($\sigma_y > 2\sigma_x$), which would not affect the neutrino event rate.

6. Beam Plug Design

As shown in Section 3, a beam plug located after the first horn in the LE configuration of the PH2 focusing system decreases the high energy tail of the neutrino spectrum. In case of mis-steered beam which misses the target, the beam plug should withstand the full intensity of the primary proton beam. Hence graphite is chosen as the material for the beam plug core. Based on neutrino beam simulations, and considering available sizes of ZXF–5Q grade cylinders, a 1.5 m (5×0.3 m) long, 31.7 mm diameter plug core was chosen [18]. This diameter is large enough to avoid an interaction of the mis-steered proton beam with elements of a plug cooling system. The general view of the beam plug design is shown in Figure 16.

Graphite rods are encapsulated with prestress of ∼4 MPa in a 0.2 mm thick stainless steel pipe. This prestress is sufficient to provide a good thermal contact between the graphite core and stainless steel pipe if the thermal expansion coefficient of the stainless steel is close to that of the graphite. Two beryllium windows complete the enclosure of the core, so that it can be maintained in a dry helium or nitrogen atmosphere. Cooling water passes through a channel formed by the addition of another, co-axial, stainless steel pipe. The gap between the pipes is equal to 2 mm, the thickness of the external pipe is 0.3 mm. As a result, in the transverse direction the plug is equivalent to a ∼18.5 mm radius graphite rod.

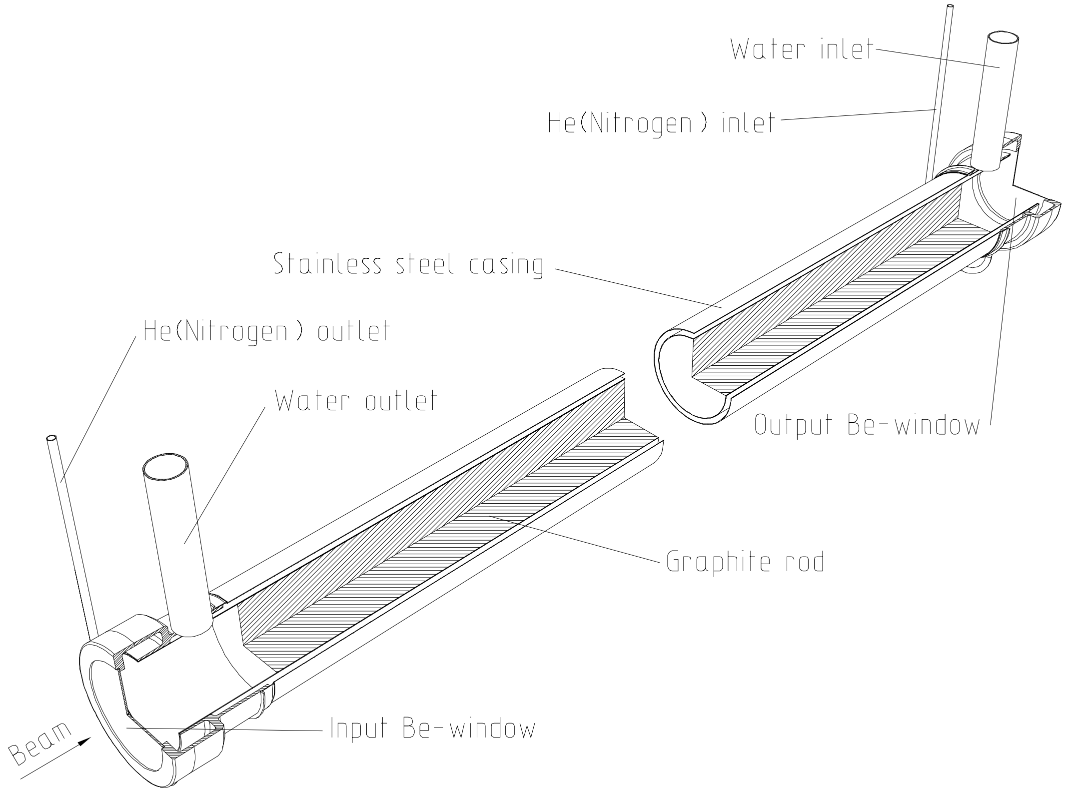

Fig. 16. General view of the beam plug design for the LE beam.

The reliability of the plug is determined by the temperature and stresses from mis-steered full intensity primary beam directly hitting the plug core. Under these conditions the total average power deposited in the graphite core is equal to 19.7 kW. Including 4.9 kW deposited in the water cooling system, the total load to a cooling system will be about 25 kW. At a water flow rate of 17 l/min and pressure drop of 1 atm, the water temperature rise will be equal to 23°C. (When a primary beam is steered properly on the target, the total heat load and water temperature rise are ∼6.4 kW and 6°C).

Calculations of the graphite core temperature were made assuming a 10 $\mathrm{kW/m^2/K}$ heat transfer coefficient to cooling water with input temperature of 20°C, and with zero heat resistance between the graphite core and stainless steel pipe. The adiabatic temperature rise and, correspondingly, quasi-static thermal stresses reach their maximal values in the cross-section with the maximal energy deposition density, which is approximately the same as in the graphite targets (see Table 6). At this location the adiabatic temperature rise ΔT and the maximal temperature T_{max} are equal to 295°C and 340°C, respectively, while the equivalent stress is about 24 MPa and corresponds to all-axis compression of the graphite. For a single turn extraction of a primary beam with $\tau \simeq 8$ μs, the maximal value of dynamic stress is about 29 MPa.

Taking into account the results of fatigue tests for graphite and the compressive strength limit of the selected graphite grade of 210 MPa (see previous Section), the safety factor is at least 4, even in the case that the mis-steered primary beam continuously hits the plug core. In a regular operation mode, when properly steered primary beam interacts with a production target, stresses in the graphite core are significantly smaller.

7. Conclusions

The proposed conceptual design of a focusing system for the Fermilab long-baseline neutrino facility provides an effective and flexible use of the 120 GeV high intensity proton beam. The design uses the same pair of horns and the same horn power supply for the production of both wide and narrow band neutrino beams, with different average energies in the 1–24 GeV energy range. Due to the higher priority of the wide band beams, the conceptual design has been carried out on all parts of that focusing system: the horns, targets and beam plug. For narrow band beams design emphasis has been on the beam optics and proton beam absorber. In conclusion :

1. The three WBB configurations described provide in the far MINOS detector neutrino beams with $E_\nu \simeq 3.5 \pm 2.5$ GeV (LE), $E_\nu \simeq 7.0 \pm 5.0$ GeV (ME), $E_\nu \simeq 14 \pm 10$ GeV (HE) and with 255, 1155, 2694 ν_μ CC events per kiloton of detector per year in these energy ranges. In addition, a WBB with any intermediate energy may be obtained by changing the target position and, for a full optimization, the position of the second horn. For these intermediate tunes, the expected number of ν_μ CC events per kton-year in the similar ±70% energy spread may be roughly estimated as $N_{CC} \simeq 230\langle E_\nu \rangle - 530$.

2. The NBB configuration provides (by means of variation of target positions and scaling of currents in dipoles) neutrino beams with $N_{CC} \simeq 31\langle E_\nu \rangle$ events per kton-year in the energy range from 4.3 to 17.2 GeV, which correspond to parent particle momenta from 10 to 40 GeV/c. The width of the NBB energy spectra is about ±15%, and may be varied somewhat by modifying the collimator in the momentum selection part of the focusing system.

3. Target designs have been developed which have a small target width to minimize reabsorption of secondaries and short segment length to minimize stresses induced by the high intensity proton beam. Both graphite and beryllium are acceptable target materials. Preference is given to graphite, which yields 8–10% higher neutrino event rates in the far detector for the ME and HE beams (for the LE beam this difference does not exceed 1–2%); beryllium is also more expensive, requires special safety measures, and ends up as a mixed waste when decommissioned.

4. Both 1 ms resonant and 8 μs single turn extractions of the primary proton beam are acceptable for target operation, although dynamic stresses arising in graphite target segments for a single turn extracted primary beam are ∼30% higher than quasi-static thermal stresses induced by a resonant extracted beam. For the latter, the safety factor (i.e. the ratio of the 10^7 cycle fatigue endurance limit to the maximal equivalent stress occurring in target segments) is equal to 2.0 and 1.6 for ME and LE graphite targets, respectively.

References

[1] The MINOS Detectors Technical Design Report, NuMI-L-337, Fermilab, 1998.

[2] G.Acquistapace et al., The West Area Neutrino Facility (WANF) for CHORUS and NOMAD Experiments, CERN-ECP/95-014, 1995.

[3] Y.Yamanoi et al., KEK Preprint 99-178 (1999).

[4] J.Dusseux, J.Pattison, G.Ziebarth, Preprint CERN 72-11, 1972.

[5] F.Nezrick, IEEE Trans. Nucl. Sci., NS-22, 1479 (1975).

[6] D.Baratov et al., Journal of Techn. Phys., 47, 1007 (1977).

[7] A.Abramov et al., Conceptual Design of NBB absorber and Low Energy WBB Calculations, NuMI-B-394, Fermilab, 1998.

[8] V.Garkusha, F.Novoskoltsev and V.Zarucheisky, The PH2M Two Horn Focusing System for the NuMI Project, NuMI-B-471, Fermilab, 1999.

[9] D.Baranov et al., Preprint IHEP 78-136, 1978.

[10] A.Abramov et al., Proc. of the XVI Russian Part. Acc. Conf., v.2, p.193-196, Protvino, 1998.

[11] M.Reichanadter et al., A High Intensity Beam Absorber Corebox for the Fermilab Main Injector Abort System, Fermilab, 1996.

[12] Ch.Iselin, Preprint CERN 74-17, 1974.

[13] J.Hylen, A.Para, GEANT based computer code developed specifically for the NuMI beam design.

[14] A.Ball, S.Katsanevas, N.Vassilopoulos, Nucl. Instr. and Meth. A383 (1996) 277-290.

[15] G.Acquistapace et al., The CERN Neutrino Beam to Gran Sasso (NGS), CERN 98-02, INFN/AE-98/05, 1998.

[16] A.Abramov et al., Advanced Conceptual Design of the Full Scale Fin Target and Engineering Design of the Target Prototypes, NuMI-B-454, Fermilab, 1998.

[17] K.Budal, Preprint CERN 67-17, 1967.

[18] A.Abramov et al., Advanced Conceptual Design of the Low Energy Target and Beam Plug, NuMI-B-543, Fermilab, 1999.

[19] Poco Graphite Inc., A Unocal Company, 1601 South State Street, Decatur, Texas 76234.

[20] Brush Wellman Inc., Engineered Materials, 17876 St. Claire Avenue, Cleveland, Ohio 44110.

[21] I.Degtyarev et al., IHEP Preprint 94-119, 1994.

[22] W.Kalbreier, W.Middelkoop, P.Sievers, CERN LAB II/BT/74-1, 1974.

[23] D.Dombrowski, E.Deksnis, M.Pick, v.5 of "Atomic and Plasma Material Interaction Data for Fusion", Int. At. En. Agency, Vienna, Austria, 1995.

[24] B.Wilkins, Journal of Materials, 7(2), 251 (1972). B.Wilkins and A.Reich, AECL-4216 (1972).

Received January 10, 2001

А.Г.Абрамов Н.А.Галяев, В.И.Гаркуша и др.
Разработка оптики пучков и конструкции мишеней для проекта NuMI.

Оригинал-макет подготовлен с помощью системы LaTeX.
Редактор Е.Н.Горина. Технический редактор Н.В.Орлова.

Подписано к печати 24.01.2001. Формат 60 × 84/8. Офсетная печать.
Печ.л. 2.75. Уч.-изд.л. 2.2. Тираж 160. Заказ 49. Индекс 3649.
ЛР №020498 17.04.97.

ГНЦ РФ Институт физики высоких энергий
142284, Протвино Московской обл.

Индекс 3649

ПРЕПРИНТ 2001-2, ИФВЭ, 2001